

# Gradient-free Post-hoc Explainability Using Distillation Aided Learnable Approach

Debarpan Bhattacharya, *Student Member, IEEE*, Amir H. Poorjam, Deepak Mittal, and Sriram Ganapathy, *Senior Member, IEEE*

**Abstract**—The recent advancements in artificial intelligence (AI), with the release of several large models having only query access, make a strong case for explainability of deep models in a post-hoc gradient free manner. In this paper, we propose a framework, named distillation aided explainability (DAX), that attempts to generate a saliency-based explanation in a model agnostic gradient free application. The DAX approach poses the problem of explanation in a learnable setting with a mask generation network and a distillation network. The mask generation network learns to generate the multiplier mask that finds the salient regions of the input, while the student distillation network aims to approximate the local behavior of the black-box model. We propose a joint optimization of the two networks in the DAX framework using the locally perturbed input samples, with the targets derived from input-output access to the black-box model. We extensively evaluate DAX across different modalities (image and audio), in a classification setting, using a diverse set of evaluations (intersection over union with ground truth, deletion based and subjective human evaluation based measures) and benchmark it with respect to 9 different methods. In these evaluations, the DAX significantly outperforms the existing approaches on all modalities and evaluation metrics.

**Index Terms**—Explainable artificial intelligence (XAI), distillation, saliency maps, object recognition, audio event classification.

## I. INTRODUCTION

In today’s machine learning, deep neural models are the mostly widely used manifestation of mapping functions from the feature space to the target labels. Current deep models with state-of-the-art capabilities consist of specialized units for processing different kinds of modalities, for example, fully connected neural networks [1], long short-term memory units [2], attention units [3], transformers [4], auto encoders [5] etc. Diverse combinations of such architectures at massive scale have manifested in the development of foundation models, with astounding performance on several tasks, for example, Vision Transformer (ViT) [6] in computer vision, Whisper [7] in speech processing and GPT-4 [8] in natural language processing. In several domains, the sequence-to-sequence models

based on transformer architecture [4] have achieved state-of-art results and in some cases elicited super-human performances.

While the models may have illustrated impressive performance, the deep complex architectures are inherently non-explainable. While knowledge distillation can provide simpler modeling solutions [9], [10], the questions about data contamination and leakage [11], as well as the over-estimation of the model performance [12], continue to be pertinent in this age of large language models (LLMs) [13]. The research direction of explainable artificial intelligence (XAI) attempts to provide solutions for this scenario.

Explainability of deep models is a crucial requirement if they are deployed in safety-critical scenarios [14]–[17]. For example, in domains like autonomous driving, finance, and healthcare, lack of explainability in the complex neural models may turn the practitioners away from exploiting the impeccable results that these models may offer. Further, XAI approaches can also help in identifying spurious correlations [18], [19] and biases [20], [21] present in the datasets and models.

### A. Types of XAI methods

The explainability problem first assumes a framework where the model (referred to as the black-box in our discussion) configuration, architecture information, and downstream tasks, are given. The setting explored in this paper is one in which an explanation is sought for an already trained black-box model with no further provision to modify/retrain it, called the *post-hoc explainability* setting. Based on different criteria, post-hoc methods can be further categorised based on,

**Model architecture:** The XAI approaches can be, (a) *Model-specific*: when the XAI method works only for a specific black-box architecture (for example, XAI for CNN-based models [22], [23]); or (b) *Model-agnostic*: when the XAI method is agnostic to the architecture of the black-box [24]–[26].

**Access to black-box:** Depending on the access requirements of the XAI methods, they can be classified as, (a) *gradient-based approaches*: XAI methods using gradient access to black-box like [23], [25], [27]; or (b) *gradient-free approaches*: XAI methods that only need input-output access without gradient access like, perturbation-based methods [26], [28], [29].

**Locality of explanations:** As the black-box is highly nonlinear, the explanation can be, (a) *local* - the methods that attempt to generate explanations for each test example like [29], [30],

D. Bhattacharya is a PhD student at the Electrical Engineering department, Indian Institute of Science, Bangalore, India, 560012. A. Poorjam<sup>†</sup> is a Data Science Specialist in Global Clinical Department at Lundbeck A/S in Copenhagen, Denmark. D. Mittal<sup>†</sup> is a PhD student at the Artificial Intelligence department, Indian Institute of Technology, Hyderabad. S. Ganapathy is an Associate Professor and the Director of the Learning and Extraction of Acoustic Pattern (LEAP) laboratory, Electrical Engineering, Indian Institute of Science, Bangalore, India.

<sup>†</sup>This work was done during employment at Verisk.

Manuscript submitted on July 7, 2023.

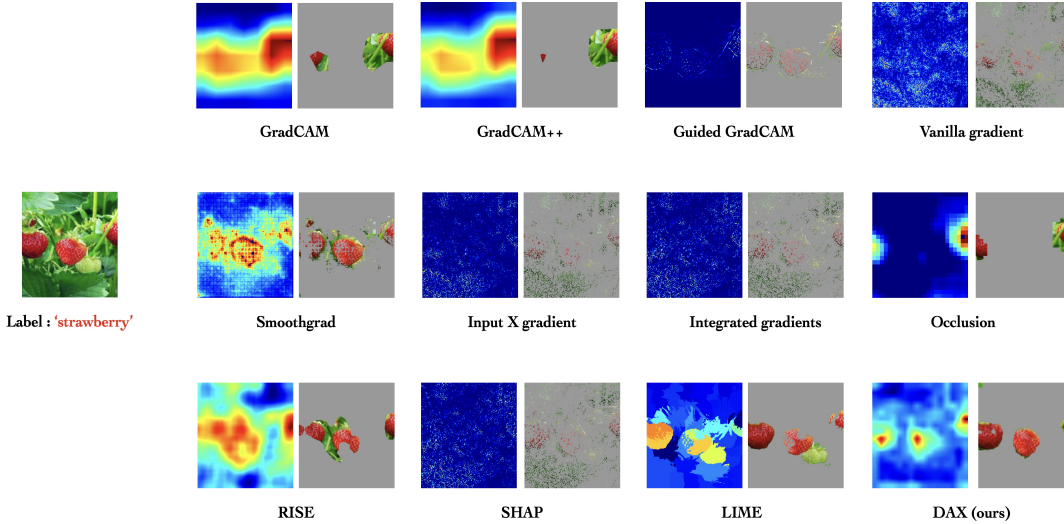


Fig. 1. Comparing various XAI methods and DAX for input *strawberry* image with the explanation heat map and the mask multiplied input.

or (b) *global* - the methods that attempt to form a complete explanation of the model function, like the works reported in [31], [32].

With the increasing number of large models being released having only query access (e.g. ChatGPT [13], DALL-E [33]), developing post-hoc gradient-free XAI approaches is crucial.

### B. Contributions from the proposed framework

In computer vision and audio based models, the input dimensionality is high,  $\mathcal{O}(10^4)$  or more. (for example, high-resolution images of size  $224 \times 224$  result in input dimension of  $4e^4$ ). To avoid dealing with such high dimensional locality, the prior works compute image segments and consider each of them as a dimension rather than the raw pixels. With this approach, the input dimensionality is reduced to  $\mathcal{O}(10^1)$ . However, explanations generated this way can be *unreliable*, *erroneous* and *imprecise* as discussed in detail in Section II-A.

We propose a novel *learnable*, distillation-based approach to post-hoc gradient-free explainability that uses two non-linear networks, a) mask-generation network and, b) student network to compute explanations. The mask-generation network selects salient parts of the local input. With the mask-multiplied input, the student network attempts to locally approximate the black-box predictions. Using a joint training framework with perturbation samples, the mask-generation network finds the salient region of the input image as the explanation.

The proposed framework, termed as distillation aided explanations (DAX), is shown to compute explanations that are better than existing approaches in various aspects, although it operates directly on the  $\mathcal{O}(10^4)$  dimensional input space of the black-box, while adding a minimal computational overhead.

This paper extends our prior work using student-teacher distillation [34]. The following are the major contributions in this paper,

- 1) Mathematical formulation of the DAX framework with the optimization.
- 2) A simplified approach which generates a single explanation mask over all the input channels.

- 3) Detailed analysis on the sensitivity of the approach as well as with samples that are incorrectly predicted by the black-box model.
- 4) Extensive comparison with 11 baseline systems on image tasks with ViT/ResNet black-box models and audio tasks with ResNet/LSTM based black-box models.
- 5) Improved performance on the IoU metric, deletion area under the curve (AUC) and subjective evaluations for both the audio and image tasks compared to all the baselines systems.

## II. RELATED PRIOR WORK

### A. Post-hoc explainability approaches

An illustration of the explainability provided by various methods for an image example is shown in Figure 1. There are several prior works using gradient access based explainability, namely,

- 1) Vanilla gradient [35], gradient $\times$ input [36], [37], smoothgrad [27] and Integrated gradients [38].
- 2) Class activation maps (CAM) [22], Gradient based class activation maps (GradCAM) [30], guided GradCAM [30], and GradCAM++ [23].

This work considers the problem of gradient-free XAI. Below, we describe the details of the prominent gradient-free XAI approaches. In this description, we use the following notation. The input is denoted as  $x_p$ , the perturbed input samples are denoted as  $\{x_p^i\}_{i=1}^Q$ , where  $Q$  denotes the number of perturbations,  $y_p^i$  denotes the output of the black-box model for the perturbed samples,  $T$  denotes the target class, and  $M$  denotes the multiplier mask.

1) *Occlusion*: Occlusion methods originated from the work on understanding neural networks [28]. It is a sliding window based approach that hides portions of the input image and studies the change in class activations to find the explanations.

2) *RISE*: Randomized Input Sampling for Explanation (RISE) [29] is another perturbation based approach, where the perturbation samples  $x_p^i$  are generated by masking out

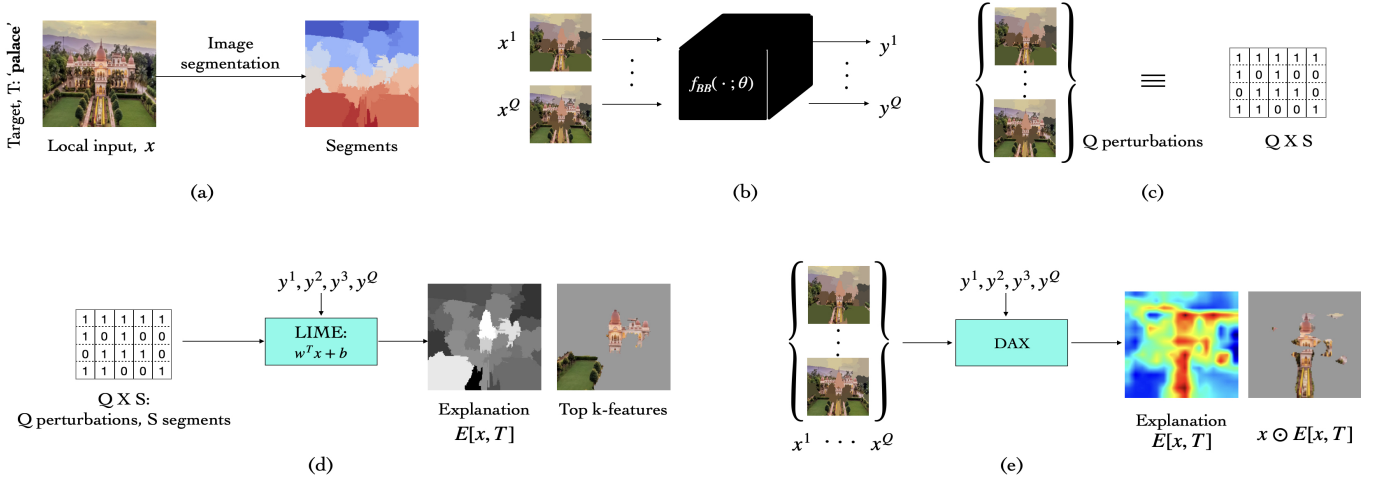


Fig. 2. Contrasting the local linear approximation approach LIME [26] for explainability and DAX (this work). (a) LIME segments the input image  $x$ . Let, the number of segments be  $S$ . (b) Then, it masks off segments randomly and generates the corresponding black-box responses,  $y^1, \dots, y^Q$  where  $Q$  is the number of perturbation samples. (c) Each of the perturbed image is represented by a binary row of size  $S \times 1$  where a 1 represents masking off the corresponding segment. (d) Using the binary matrix of size,  $Q \times S$  as input, and  $y^1, \dots, y^Q$  as targets, the LIME fits a linear model. Following the training, the linear weights denote the explanation of the input, in terms of weights corresponding to the segment locations. (e) DAX, in contrast, operates on the image space directly and uses non-linear local approximation to generate the explanation.

the input image using randomly generated binary masks. The masked image samples are passed through the black-box and the corresponding black-box scores for the target class  $[y_p^i]_T$  are stored. The final explanation  $E_{rise}(x_p, T)$  is computed as,

$$E_{rise}(x_p, T) = \frac{\sum_{i=1}^Q x_p^i [y_p^i]_T}{\sum_{i=1}^Q [y_p^i]_T} \quad (1)$$

3) **SHAP**: SHapley Additive exPlanations [39] is a game theoretic approach to explainability. It computes shapely values as explanation and proves the uniqueness of the solution. Their formulation assumes the explanation itself as a model, which is called as the explanation model.

4) **LIME**: Local Interpretable Model-agnostic Explanations (LIME) [26] is based on the popular approximation in the perturbation based methods - the local linear approximation. The local linear approximation provides explanation by exploiting two facts - a) the linear regression model is inherently interpretable, and b) the non-linear function can be approximated as a linear one within the local neighbourhood. The working details of the LIME model are shown in Figure 2. LIME first perturbs the local input to generate numerous neighbourhood samples, computes the corresponding black-box responses using the query access to black-box, and fits a linear regression model using the mask and responses as inputs and targets, respectively.

The LIME approach has three major drawbacks, which we attempt to address in the proposed DAX framework.

**Limitations of linear approximation**: If the locality of black-box function near an input is not smooth, as shown in Figure 3, the explanations are generated from an invalid approximation of the black-box model. A potential solution to overcome this scenario is to allow the local approximation to be non-linear. In the proposed DAX setting, we have designed a student network to approximate the local behavior. As shown in Figure 3(b), even a mildly non-linear approximation can mitigate the approximation error to a large extent.

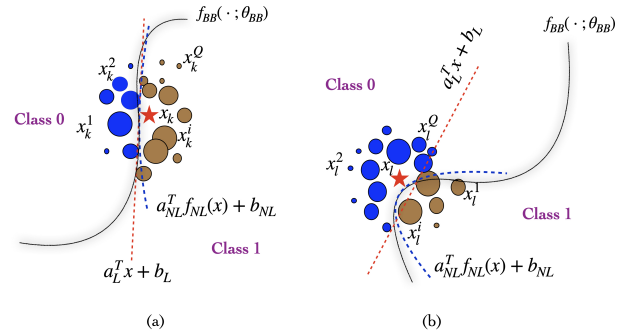


Fig. 3. Let  $f_{BB}(\cdot; \theta_{BB})$  be the trained black box neural network whose decision boundary (separating two classes) is shown by black solid lines in the figure. The decision boundary has different local curvatures near local inputs  $x_k$  (figure (a)) and  $x_l$  (figure (b)). (a) Locally linear assumption (red dashed line) is a good approximation of the black box at  $x_k$ . (b) As the decision boundary is less smooth near  $x_l$ , a linear assumption (red dashed line) is a bad local approximation of the black-box. A mild non-linearity (blue dashed line) can significantly reduce the approximation error.

**Input data manifold**: Images are associated with very high dimensionality ( $\mathcal{O}(10^4)$  for 224 X 224 image). Local linear approximations are cumbersome to model on such high dimensional sub-spaces. As a way around, LIME segments the input image, and uses the segment locations as the input variables without working on the pixels. This leads to a drastic reduction in the input dimensionality of  $\mathcal{O}(10^1)$ . The LIME [26] fits a linear model using binary information about masking (if a segment is masked-off or not), as shown in Figure 2. This may bring the reliability of the explanations into question. Narodytska et al. [40] argues that the LIME generated explanations may not be accurate as it operates on a reduced subspace of the local input. In the proposed DAX framework, we attempt to overcome this issue by directly operating on the raw input image space.

**Imprecise explanations**: The explanation importance weights are obtained at the segment level. This may lead to imprecise explanations, as shown in Figure 2(d). In the proposed DAX

framework, the explanations are obtained at the pixel level, making them very precise. We also use the segment-anything-model (SAM) [41] to generate precise segments that can be used for the XAI setting.

### III. METHODOLOGY

#### A. Problem formulation

We formalize the problem in a supervised classification setting. Let,  $f_{BB}(\cdot; \theta_{BB})$  denote a trained deep neural network based classifier (black-box), which is to be explained. The training dataset is denoted as  $\{x_i \in X \sim D_X, z_i \in Z \sim D_Z\}_{i=1}^N$ , with  $x_i \in \mathcal{R}^D$  as inputs, and  $z_i \in \mathbb{Z}$  denoting the one-hot labels. The pre-trained model parameters are denoted as  $\theta_{BB}$ , with  $C$  classes. Thus, the model  $f_{BB}(\cdot, \theta_{BB})$  has  $C$  output nodes with softmax non-linearity,

$$|y| = |f_{BB}(x; \theta_{BB})| = C; \quad \sum_{i=1}^C [f_{BB}(x; \theta_{BB})]_i = 1, \quad \forall x \quad (2)$$

The problem of explaining the black-box is defined for a given input  $x_p$ . For the target-class  $T$ , the goal is to explain the prediction  $[y_p]_T$ , given  $x_p$ , where  $y_p = f_{BB}(x_p; \theta_{BB})$ .

#### B. Functional view of “explanation”

We pose explanation for the black-box as a function,

$$E[x_p, T] = E(x_p, y_p | f_{BB}(\cdot; \theta_{BB}), T) \in \mathcal{R}^D \quad (3)$$

where  $E[x_p, T]$  denotes an explanation computed on  $x_p$ , in the form of weights assigned to each dimension of  $x_p$  for the prediction of the target-class  $T$ , denoted as  $[y_p]_T$ . In particular,  $E[x_p, T] \in \mathcal{R}^D$  denotes a saliency map (also referred to as explanation mask), where  $[E[x_p, T]]_k$ , denotes the importance of  $k$ -th dimension of  $x_p$  in generating the prediction,  $[y_p]_T$ .

1) *Neighbourhood sampling*: To generate the explanation for a local input,  $x_p$ , our approach relies on neighbourhood samples at close proximity of  $x_p$ , obtained by perturbing  $x_p$ . As pointed out by Fong et. al. [42], the perturbations must be “meaningful” (having contextual meaning). For images, segmentation [43] is an algorithm that captures contextual meaning. Hence, we perturb image segments to obtain neighbourhood samples - similar to the perturbation strategy used by LIME [26]. Let, the local input  $x_p$  contain  $S$  segments  $\{u_1, u_2, \dots, u_S\}$  obtained using an image segmentation algorithm. The segments are non-intersecting and exhaustive.

$$u_i \in x_p \quad \forall i; \quad u_i \cap u_j = \phi, \quad i \neq j; \quad \bigcup_{i=1}^S u_i = x_p \quad (4)$$

For generating  $Q$  neighbourhood samples,  $x_p$  is randomly perturbed  $Q$  times by randomly masking off a subset of the segments  $\{u_i\}_{i=1}^S$ . Let the neighbourhood samples be denoted as  $\{x_p^i\}_{i=1}^Q$ , with the  $i$ -th sample  $x_p^i$  containing only a subset of the segments. Let the mask of indices be denoted by  $I_i \in \mathbb{Z}^{S \times 1}$ , where  $[I_i]_j = \mathbb{1}_{\{j\text{-th segment is masked-off}\}}$ . Thus, the  $i$ -th neighbourhood sample of  $x_p$  is given by,

$$x_p^i = \bigcup_{\substack{j=1 \\ [I_i]_j=0}}^S u_j \quad (5)$$

It is noteworthy that existing local approximation methods [26] use the low dimensional  $I_i$  as inputs to the local approximation model (Figure 2). In contrast, our approach directly operates on data samples,  $x_p^i$ , to generate the explanation.

2) *Explanation strategy*: The problem is to find the explanation  $E[x_p, T]$  given  $Q$  neighbourhood samples  $\{x_p^i\}_{i=1}^Q$ , query access to  $f_{BB}(\cdot; \theta_{BB})$ , and the target-class  $T$ .

**The learnable distillation approach** : Our approach has two learnable components - a *mask generation network* and a *student network*. The job of the mask generation network is to find the salient regions in the image (the explanation), while the student network tries to locally distill the black-box.

#### C. DAX framework

1) *“Explanation” as the optimal multiplier*: We look at the notion of explanation as an optimal multiplier of the input that causes minimum drop in the black-box prediction of the target-class. The true explanation,  $E^*[x_p, T]$ , assigns higher weights to the dimensions of  $x_p$  that are most important for the model,  $f_{BB}$ , to make the target-class prediction  $[y_p]_T$ . If  $M_p^T \in \mathcal{R}^D$  is any input multiplier and  $0 \leq [M_p^T]_k \leq 1 \quad \forall k$ , then we obtain the optimal multiplier,  $M_p^{T*}$ , with the optimization,

$$E^*[x_p, T] = M_p^{T*} = \arg \min_M ([y_p]_T - f_{BB}(M \odot x_p; \theta_{BB}))^2 \quad (6)$$

Equation (6) poses the problem of finding the explanation as a learnable approach, where explanations can be found by minimizing the mean squared error (MSE) between black-box output for the original input and the black-box response for the “perfectly” masked input.

2) *Distillation to avoid gradient flow restriction*: Using the perturbation samples  $\{x_p^i\}_{i=1}^Q$  and corresponding black-box responses  $\{[y_p^i]_T\}_{i=1}^Q = \{[f_{BB}(x_p^i; \theta_{BB})]_T\}_{i=1}^Q$ , one can optimize the explanation motivated by Equation (6).

However, in a gradient-free setting, gradient flow through black-box model is not available. In order to perform the optimization described above without gradient-access, we propose a student distillation model, which locally approximates the black-box model. In this way, the distilled network can be used for learning the explanation, as the gradients can be computed.

Thus, we have two optimization problems at hand - i) Finding a local approximation of the black-box using distillation and, ii) Finding a multiplier based explanation (Equation 6). We perform a joint optimization of these two sub-problems, as described in the following sub-sections.

3) *Local distillation of black-box*: The black-box is locally distilled by approximating the black-box behavior at the vicinity of local input,  $x_p$ . The neighbourhood samples  $\{x_p^i\}_{i=1}^Q$  and black-box responses  $\{[y_p^i]_T\}_{i=1}^Q$  are used to train a small learnable network,  $f_S(\cdot; \theta_S)$ , where  $\theta_S$  denotes the model parameters of the student network. We minimize the MSE loss to learn the parameters of the student network,  $f_S(x_p^i; \theta_S)$ , i.e.,

$$\theta_S^* = \arg \min_{\theta_S} \sum_{i=1}^Q ([y_p^i]_T - [f_S(x_p^i; \theta_S)]_T)^2 \quad (7)$$

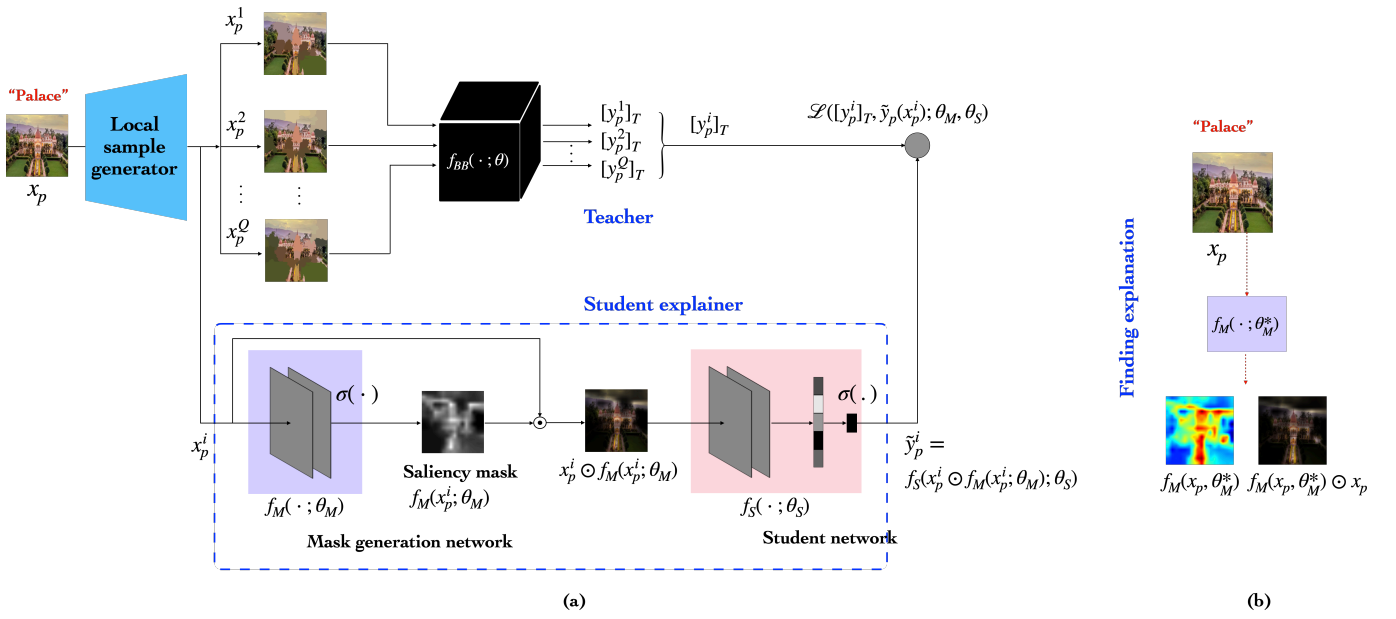


Fig. 4. The DAX framework. In part (a), we show the two components of the model, which are highlighted in the bottom row - i) Mask generation network, and ii) Student network. In part (b), the inference step is illustrated.

4) *Learnable explanation*: Interestingly, as seen in Equations (6) and (7), finding the explanation and local distillation are posed as the minimization of objective functions based on the MSE loss. We propose to combine the two optimization problems with two learnable networks, a mask generation network,  $f_M(\cdot; \theta_M)$  and a student network,  $f_S(\cdot; \theta_S)$ . Now, minimization of the following loss

$$\mathcal{L}_{\text{MSE}}(x_p^i, T; \theta_M, \theta_S) = \left[ [y_p^i]_T - f_S(x_p^i \odot f_M(x_p^i; \theta_M)); \theta_S \right]^2 \quad (8)$$

allows the estimation of the parameters  $\{\theta_M, \theta_S\}$ . Here,  $f_M(x_p; \theta_M)$  is the multiplier mask generated by the mask generation network, while the product,  $x_p \odot f_M(x_p; \theta_M)$ , is the salient explanation output of the proposed DAX framework. Let  $\tilde{y}_p(x_p^i) = f_S(x_p^i \odot f_M(x_p^i; \theta_M); \theta_S)$  denote the output of the DAX model for the perturbed input  $x_p^i$ .

Note that, optimizing based on Equation (8) can be ill-posed, as it can lead to the trivial identity solution  $f_M(x_p; \theta_M) = \mathbb{I}$ . It can be avoided by using a regularized loss. We propose an  $\mathbb{L}_1$  loss, as discussed in Equation (10) given below.

$$\{\theta_M^*, \theta_S^*\} = \arg \min_{\theta_M, \theta_S} \mathcal{L}_{\text{TOTAL}}(x_p, T; \theta_M, \theta_S) \quad (9)$$

$$\mathcal{L}_{\text{TOTAL}}(x_p, T; \theta_M, \theta_S) = \sum_{i=1}^Q \gamma_i \mathcal{L}_{\text{MSE}}(x_p^i, T; \theta_M, \theta_S) + \lambda_1 \mathcal{L}_{\text{SP}}(x_p^i; \theta_M) + \lambda_2 \mathcal{L}_{\text{KL}}(x_p^i; \theta_M, \theta_S) \quad (10)$$

where,

$$\mathcal{L}_{\text{SP}}(x_p^i; \theta_M) = \sum_{i=1}^Q \|f_M(x_p^i; \theta_M)\|_{\mathbb{L}_1} \quad (11)$$

$$\mathcal{L}_{\text{KL}}(x_p^i; \theta_M, \theta_S) = \mathcal{KL} \left( \mathbf{q}_{\{[y_p^i]_T\}_{i=1}^Q} \parallel \mathbf{q}_{\{\tilde{y}_p(x_p^i)\}_{i=1}^Q} \right)$$

The first term of the total loss is the MSE loss (defined in Equation (8)), the second term is the  $\mathbb{L}_1$  penalty loss

on the mask explanations, and the third term is the  $KL$ -divergence between distribution ( $\mathbf{q}$ ) of black-box model scores ( $\{[y_p^i]_T\}_{i=1}^Q$ ) and the distillation output scores ( $\{\tilde{y}_p(x_p^i)\}_{i=1}^Q$ ).

The  $KL$ -divergence loss helps in bringing the distributions of DAX scores closer to the black-box scores, which regularizes the MSE loss. The  $\gamma_i$  weighs the ‘‘closeness’’ of the neighbourhood samples to the actual input  $x_p$ , i.e.,  $\left( \gamma_i \propto \frac{1}{\|x_p - x_p^i\|_{L_2}} \right)$ . Further,  $\tilde{y}_p(x_p^i)$  is defined in the description below Equation (8), and  $\lambda_1, \lambda_2$  are hyper-parameters that are set based on a held-out validation set.

The distribution  $\mathbf{q}$  is computed at a batch-level using a histogram. The optimization of the total loss is performed in iterative fashion using gradient descent. The neighbourhood samples are divided into training and validation set following standard machine learning protocols. In our experiments, the number of local neighbourhood samples and batch size used for DAX saliency learning are 6000 and 64, respectively. Also, the hyper-parameters  $\lambda_1$  and  $\lambda_2$  are selected as 0.001 and 0.02 respectively, based on experiments on the validation set.

We have also experimented with a quadratic counterfactual loss for encouraging sparsity, instead of the  $\mathcal{L}_{\text{SP}}(x_p^i; \theta_M)$ . It minimizes the agreement between the student model scores and the black-box scores when the mask  $f_M(x_p^i; \theta_M); \theta_S$  is complemented.

$$\mathcal{L}_{\text{CNT}}(x_p^i, T; \theta_M, \theta_S) = \left( [y_p^i]_T - f_S(x_p^i \odot f_M^C(x_p^i; \theta_M)); \theta_S \right)^2$$

where,

$$f_M^C(x_p^i; \theta_M) = (\mathbf{1} - f_M(x_p^i; \theta_M)), \quad \mathbf{1}_{ij} = 1, \forall i, j \quad (12)$$

In our experiments,  $\mathcal{L}_{\text{CNT}}$  is seen to be superior to  $\mathcal{L}_{\text{SP}}$ , resulting in significantly better performance on all the metrics, even in absence of  $\mathcal{L}_{\text{KL}}$ . Different variants of DAX loss function that are used in experiments is listed in Table I.

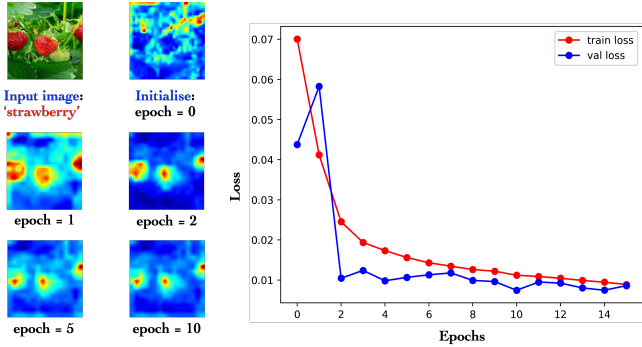


Fig. 5. The learnable explanation converges in less than 10 epochs. The (left) panel shows the mask generated in different epochs, and (right) panel shows the training and validation loss curves.

#### D. Model architecture

We use a two layer convolutional network (CNN) with sigmoid activation for mask generation network,  $f_M(\cdot; \theta_M)$ . The student network,  $f_S(\cdot; \theta_S)$  consists of 2 CNN layers followed by a fully-connected layer with sigmoid activation, as shown in Figure 4.

The sigmoid function at the output of  $M = f_M(\cdot; \theta_M)$  ensures that the mask multiplier satisfies  $M_{ij} \in [0, 1]$ , while the sigmoid activation at the output of the student network ensures that the distilled scores ( $\tilde{y}_p$ ) and the target scores  $y_p$  are in the same numerical range.

After the training is complete, the explanation can be obtained as,

$$E[x_p, T] = x_p \odot f_M(x_p; \theta_M) \quad (13)$$

and the student network  $f_S(\cdot; \theta_S^*)$  can be discarded. The steps to find the explanation<sup>1</sup> using proposed approach are outlined in Algorithm 1.

---

#### Algorithm 1: Finding explanation

---

**Inputs:**  $f_{BB}(\cdot; \theta_{BB})$ ,  $x_p$ ,  $T$

**Output:**  $E[x_p, T]$

**Training:** Initialization:

$\{n, Q\} \leftarrow \{\text{no. of epochs, no. of perturbations}\};$

$\{\theta_H, \theta_D\} \leftarrow \text{random};$

$epoch \leftarrow 0$

Obtain  $\{x_p^i\}_{i=1}^Q$  and

$\{\{y_p^i\}_T\}_{i=1}^Q = \{\{f_{BB}(x_p^i; \theta_{BB})\}_T\}_{i=1}^Q$

**while**  $epoch \ k \leq n$  **do**

    Compute  $f_M(x_p^i; \theta_M)$  ;

    Compute  $\tilde{y}_p(x_p^i) = f_S(x_p^i \odot f_M(x_p^i; \theta_M); \theta_S)$  ;

    Compute  $\mathcal{L}_{TOTAL}$  using Equation (10);

$(\theta_M, \theta_S)^{(k)} \leftarrow (\theta_M, \theta_S)^{(k-1)} - \eta \nabla \mathcal{L}_{TOTAL}^{(k-1)}$  ;

$k = k + 1$ ;

**end**

**Inference:**  $E[x_p, T] = x_p \odot f_M(x_p; \theta_M)$

---

We also explore the application of segment-anything-model (SAM) [41] as the segmentation algorithm for the proposed

<sup>1</sup>The implementation of the DAX model is available in <https://github.com/iiscleap/DAX>

DAX variants	Components	
	Segmentation algo.	Loss
V1	Quick shift [43]	$\mathcal{L}_{MSE} + \lambda_1 \mathcal{L}_{L1} + \lambda_2 \mathcal{L}_{KL}$
V2	Quick shift [43]	$\mathcal{L}_{MSE} + \lambda_3 \mathcal{L}_{CNT}$
V3	SAM [41]	$\mathcal{L}_{MSE} + \lambda_4 \mathcal{L}_{CNT}$

TABLE I  
DIFFERENT VARIANTS OF DAX FORMULATION STUDIED.

DAX framework. The SAM framework consists of an image encoder, an optional prompt encoder and a mask decoder. We have used the SAM setup without any prompts and used the segmentation maps to generate perturbations. The different variants of the proposed DAX framework are mentioned in Table I. The epoch-wise progression of mask generation and the corresponding loss curves are shown in Figure 5, for the example image of strawberry. The saliency explanation converges quickly, within 10 epochs. The epoch-wise loss values on training and validation sets are also shown.

## IV. RESULTS

### A. Computer vision: object classification task

1) *Qualitative analysis:* We present a diverse set of input images and the compute saliency explanations to enable extensive qualitative analysis. We compare the DAX explanations with those generated by 11 other popular XAI approaches, belonging to 3 different categories, to allow a strong benchmark comparison. For this analysis, the inputs that were correctly predicted by the black-box were considered.

**Task:** The object detection task is considered for this analysis. Given an input image, the task is to predict the class of the object present in the image. Images are randomly selected from the evaluation set of ImageNet dataset [44].

**Black-box:** To analyze the explainability of the state-of-the-art models, a vision transformer [45] of patch size 16 (ViT-b16) is used as the black-box model, which was pre-trained on the ImageNet dataset. Figure 6 shows the explanations generated by our approach and 11 other popular XAI approaches. As seen here, the DAX model is able to generate consistent explanations for most of the classes shown here.

2) *Quantitative analysis:* Most of the prior explainability works only report the qualitative analysis on a selected subset of images. While this may provide visual insight, the statistical justification of the explanation quality is lacking. In this paper, we also present statistical performance of our approach on a large dataset. For extensive benchmark comparisons, we also evaluate 11 other existing methods in the same setting.

**Task:** We use the Pascal visual object classification (VOC) dataset [46], comprising of images with 20 object classes. It has two sub-parts - classification dataset (larger set having 5717 images) and segmentation dataset (smaller set having 1464 images). The images in the segmentation dataset also have the human annotated ground truth segmentation masks corresponding to the objects. We use the classification dataset for fine-tuning the models, while the segmentation dataset is used in our evaluations.

**Black-box:** We perform the statistical analysis separately on two different black-box models to analyze the performance consistency, a) The ResNet-101 [47] and, b) the ViT-b16 [45].

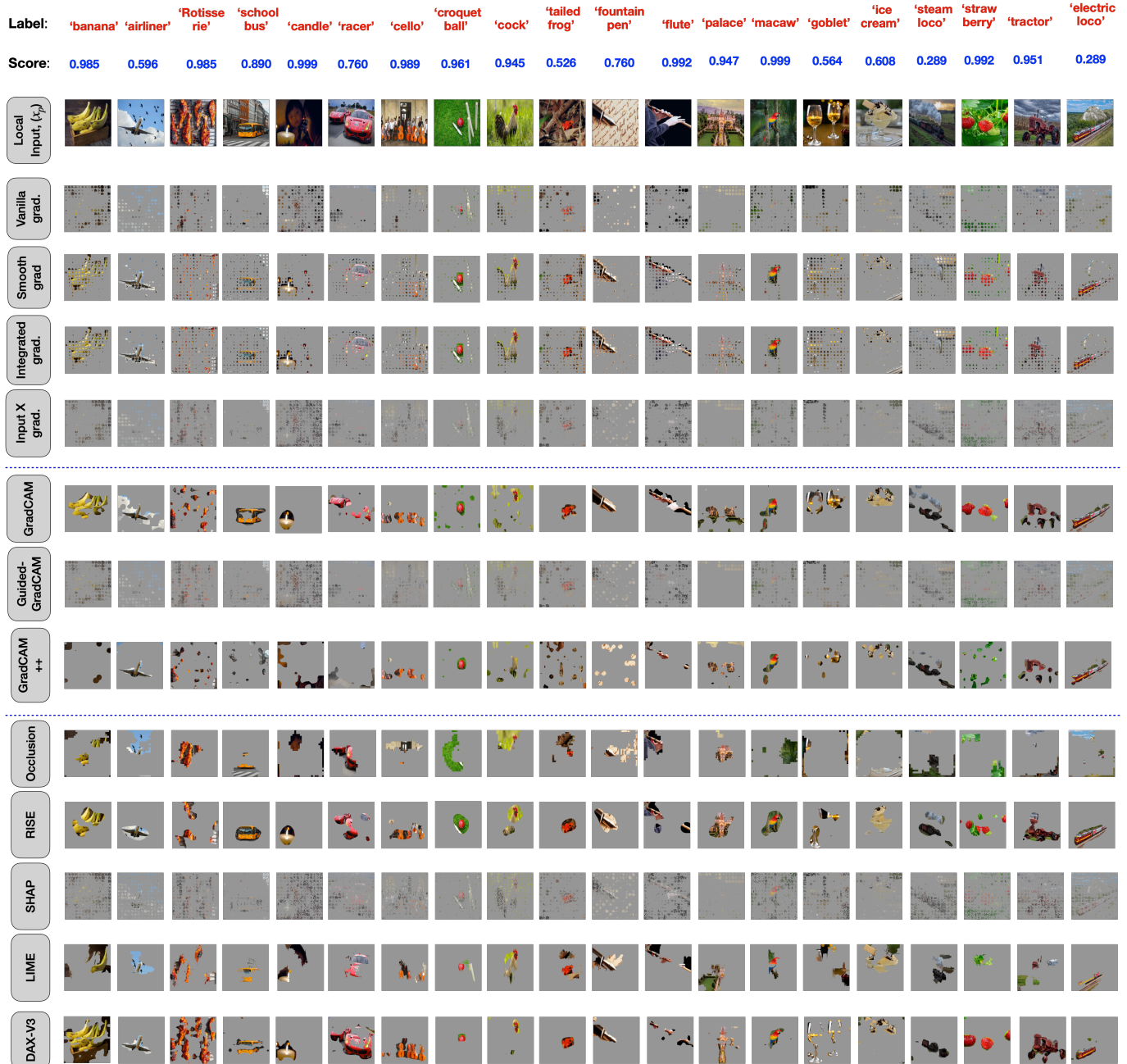


Fig. 6. Comparison of explanations generated by DAX and 11 other existing approaches for the ViT-b16 black-box model on the ImageNet dataset.

Both the black-box models are pre-trained on ImageNet [44]. We fine-tuned the black-box models on classification dataset of Pascal VOC, with 20 classes. After fine-tuning, the ResNet-101 and ViT-b16 achieved an accuracy of 86.0% and 91.2%, respectively on the segmentation set.

**Metric of explanation - IoU:** The intersection-over-union (IoU) metric is used to quantify the explanation quality. We use the ground truth object segmentation and compare this with the mask generated by the model ( $M = f_M(\cdot; \theta_M)$ ). For this IoU computation, the mask  $M$  is converted to a binary level by thresholding it. A threshold of  $\mu_M + \sigma_M$  is used for the purpose, where  $\mu_M$  and  $\sigma_M$  are the mean and standard deviation of the values in the matrix  $M$ , respectively. The IoU metric reflects how much the generated explanations aligns

with human annotated ground truth of the object classes.

**Metric of explanation - Deletion AUC:** we also computed the deletion AUC performance (proposed in RISE [29]) as the metric. In this setting, the salient regions of the image, provided by the XAI method, are masked away and the masked image is used as input to the black-box model. The masking is performed progressively with descending order of importance of regions provided by the XAI method. The final masked input corresponds to removing the entire saliency region identified by the XAI method. The drop in target class accuracy, for each level of masking, is measured. The receiver-operating-curve (ROC) is computed with the percentage of masking against the drop in target class accuracy. A lower

XAI Methods			Black box network			
			ResNet 101		ViT-base-16	
Name	Gradient free	Model agnostic	Mean IoU (%) (↑)	Mean IoU (%) on incorrect label (↓)	Mean IoU (%) (↑)	Mean IoU (%) on incorrect label (↓)
Vanilla gradient [35]	×	✓	24.8 (8.1)	0.5e-1	19.6 (5.3)	0.6e-1
Smooth-grad [27]	×	✓	34.5 (11.7)	1.1e-1	20.6 (6.4)	0.8e-1
Integrated gradients [25]	×	✓	20.1 (8.5)	1.1e-1	19.3 (15.4)	1.3e-1
Input x gradient [37]	×	✓	19.9 (8.7)	0.3e-1	19.2 (15.4)	0.5e-1
GradCAM [30]	×	×	39.6 (13.9)	2.8e-1	17.1 (11.9)	2.6e-1
Guided GradCAM [30]	×	×	19.0 (10.1)	0.8e-1	19.2 (15.4)	0.5e-1
GradCAM++ [23]	×	×	39.7 (14.0)	2.9e-1	10.5 (7.7)	2.6e-1
Occlusion [28]	✓	✓	29.6 (11.7)	3.5e-1	28.5 (12.1)	3.4e-1
RISE [29]	✓	✓	33.7 (11.5)	4.5e-1	31.1 (11.8)	4.1e-1
SHAP [39]	✓	✓	22.4 (9.3)	1.5e-1	19.3 (10.3)	1.2e-1
LIME [26]	✓	✓	29.2 (10.9)	3.2e-1	26.8 (11.4)	4.0e-1
<b>DAX-V1</b>	✓	✓	33.3 (12.1)	2.8e-1	31.4 (11.9)	3.1e-1
<b>DAX-V2</b>	✓	✓	34.7 (11.9)	2.7e-1	32.5 (11.5)	3.1e-1
<b>DAX-V3</b>	✓	✓	<b>36.9 (11.6)</b>	2.5e-1	<b>34.1 (8.9)</b>	3.5e-1

TABLE II

THE INTERSECTION-OVER-UNION (IOU) (%) WITH ASSOCIATED STANDARD DEVIATION RESULTS FOR 11 BASELINE APPROACHES AND THE PROPOSED DAX FRAMEWORK ON 1246 (AND 1321) IMAGES, WHICH WERE CORRECTLY CLASSIFIED BY THE BLACK-BOX RESNET-101 (AND ViT-B16) MODEL. THE PROPERTIES OF THE XAI METHODS ARE ALSO HIGHLIGHTED, AND THE IOU FOR RANDOMISED INCORRECT LABELS ARE ALSO GIVEN.

value of deletion AUC is preferable. Table III illustrates that the deletion AUC is the best for the the proposed method (DAX-V3), similar to the trends seen with the IoU metric.

**Explanation accuracy:** Table II shows the statistical performance of our approach and 11 other popular XAI approaches on the segmentation dataset of Pascal VOC. The analysis is performed on a total of 1246 and 1321 images for the ResNet-101 and ViT model respectively, belonging to the 20 classes, which were correctly classified by the black-box model. Our approach, that attempts to overcome limitations of LIME, is seen to achieve significant improvements (4.1% in terms of mean IoU accuracy over LIME).

**Subjective evaluation:** we performed two sets of subjective listening tests to allow robust evaluation of the XAI models.

- 1) In the first evaluation, we performed a passive task, where human participants visualized the original image with the ground-truth target class. They were tasked to rate the different XAI saliency maps in terms of explaining the target object in the given image. The saliency maps of different XAI methods were presented in random order. The mean opinion score (MoS) for the different XAI models with 30 human subjects is shown in Fig. 7.
- 2) In the second evaluation, an active human study was conducted according to the guidelines mentioned in human interpretability of visual explanations (HIVE) [48]. In this setup, shown in Fig. 8, the original image with the saliency maps are shown and the raters are asked to predict the object class that best describes the saliency map generated by the chosen XAI method. The rating is compared with the ground truth class and the prediction accuracy with respect to the target class is used as measure of the subjective quality of the XAI.

In these studies, both the DAX frameworks are consistently seen to improve over the prior works (statistically significant

XAI methods	Deletion-AUC (↓)	
	ResNet-101	ViT-base-16
Occlusion	0.351 (0.002)	0.370 (0.003)
RISE	0.323 (0.002)	0.332 (0.002)
SHAP	0.341 (0.004)	0.361 (0.003)
LIME	0.335 (0.006)	0.340 (0.005)
DAX-V1	0.318 (0.004)	0.326 (0.004)
DAX-V2	0.309 (0.004)	0.315 (0.004)
DAX-V3	<b>0.298 (0.003)</b>	<b>0.302 (0.002)</b>

TABLE III

THE MEAN AREA-UNDER-CURVE (AUC) FOR THE DELETION CURVES OBTAINED FOR VOC DATASET FOR USING DIFFERENT XAI METHODS.

improvements confirmed with a pairwise t-test, with  $p < 0.05$ ). Further, DAX-V3 is seen to outperform the DAX-V1 setting.

In terms of benchmark comparison, for ResNet model, many of the gradient-access based approaches generate good IoU values (Table II). The highest IoU is obtained using GradCAM++, which is a specially designed method for CNN based models using gradient-access. Among the model-agnostic gradient-free methods, RISE and DAX approach perform better than all the other approaches.

However, for ViT black-box, which is a attention based architecture, all the gradient-based methods elicit a significant degradation in IoU values. The DAX approach performs the best among the 12 methods compared here. It provides a 4.6% IoU gain over the LIME approach.

**Explanation sensitivity:** The explanation for a black-box is sought for a target-class  $T$ . The explanations should significantly change if  $T$  changes, a measure we call as *sensitivity* of explanations. To quantify this, while seeking explanations, we randomly pick one of the incorrect classes. In such a scenario, a lower IoU value is preferred, as this would indicate a discriminative explanation. In Table II, the DAX framework is seen to provide improved sensitivity over the RISE approach.



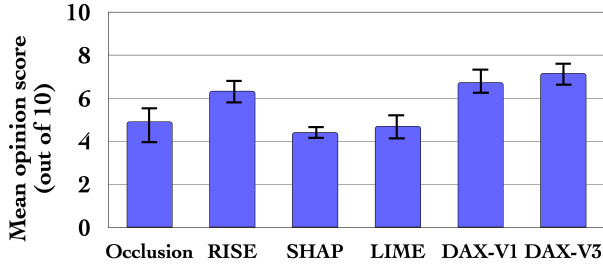


Fig. 7. Mean human opinion score (scale of 10) for the explanation quality among different XAI approaches collected from 30 subjects, with each subject visualizing 25 different image examples. DAX-V1 and DAX-V3 were preferred over others statistically significantly ( $p < 0.05$  in paired t-test).

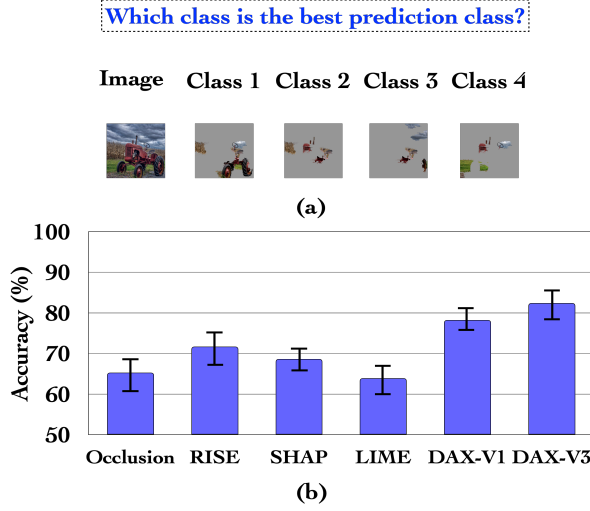


Fig. 8. The end-user utility study carried out for 6 XAI methods according to HIVE [48] guidelines. The study consists of 30 human subjects. (a) An example of the questions provided to the subjects, and (b) Average accuracy of predicting the target class using the XAI map.

DAX variants	Hyperparameters	IoU
V1	4000, 0.001, 0.01	28.5
	4000, 0.001, 0.02	29.7
	4000, 0.001, 0.04	29.5
	6000, 0.001, 0.02	<b>31.4</b>
	6000, 0.01, 0.02	30.9
	6000, 0.0001, 0.02	29.2
V2	4000, 0.1	28.3
	4000, 0.5	30.8
	6000, 0.5	<b>32.5</b>
V3	4000, 0.1	30.5
	4000, 0.5	32.9
	6000, 0.5	<b>34.1</b>

TABLE IV

ABLATION EXPERIMENTS FOR THE HYPERPARAMETER CHOICES OF DAX VARIANTS USING THE ViT BLACK-BOX MODEL.

3) *Ablation studies*: For the image processing task, we conducted several ablation studies to understand the importance of different modeling choices made in DAX framework. **Number of perturbation samples and loss weight**: For the different DAX versions, we performed an ablation study with different values of  $(Q, \lambda)$  and these are reported in Table IV. It is seen that 6000 perturbation samples, with a  $\lambda = 0.5$  provides the best IoU results for both DAX-V2 and DAX-V3

Baselines	ResNet-101	Vit base-16
DAX-Base1: stu. ntw. + RISE	31.6	31.3
DAX-Base2: student network + LIME	29.1	26.4
DAX-V2: mask-gen. + stu. ntw.	<b>34.7</b>	<b>32.5</b>

TABLE V

IOU COMPARISON BETWEEN DAX AND VERSIONS WHICH COMBINE STUDENT NETWORK DISTILLATION AND EXISTING XAI METHODS OF LIME/RISE FOR THE OBJECT CLASSIFICATION TASK WITH ViT BLACK-BOX.

DAX student architecture	ResNet-101	Vit base-16
2 CNN + 1 FCN layers	34.8	31.9
2 FCN layers	35.5	33.7
2 CNN + 2 FCN layers	<b>36.9</b>	<b>34.1</b>

TABLE VI

ARCHITECTURAL CHOICES OF STUDENT NETWORK OF DAX

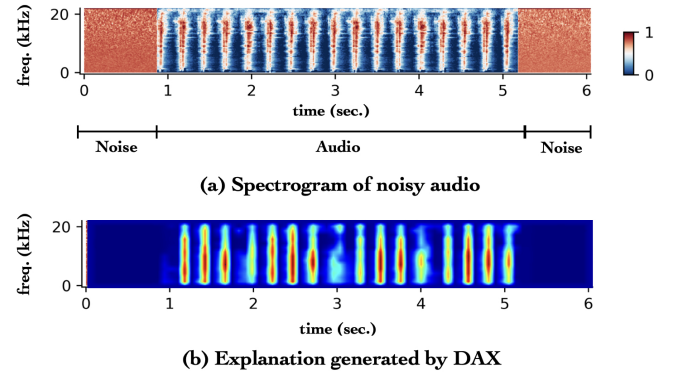


Fig. 9. The explanation generated by DAX for audio spectrogram in the audio classification task. The explanation is not affected by the added noise at both sides of the audio.

methods.

#### Using student distillation with existing XAI approaches:

We explore the option of developing a local distillation using a student model and performing LIME/RISE based explanations on these student models. This is compared with the proposed DAX setting, where both the student and explanation models are jointly optimized. The comparison, shown in Table V, highlights that the joint optimization in DAX setting gives the best IoU results over these other modeling choices.

**Model architecture**: Different configuration of fully connected or CNN architectures are explored for constructing the DAX model. These results are reported in Table VI.

#### B. Audio processing: sound event classification task

**Task**: We take up a sound event classification task, where the task is to classify an audio signal among 10 classes.

**Dataset**: We use Environmental Sound Classification (ESC-10) [49] dataset that has 10 classes of sounds.

**Black-box**: We use a ResNet-101 model for this task. The black-box was trained on spectrogram features of audio samples in the training split of ESC-10 before performing the explainability analysis on the test set of ESC-10, having 150 audio samples from 10 classes. The model accuracy was 92.7% and the explainability analysis was performed on correctly predicted 139 samples from the test set.

XAI Methods	Mean IoU (%) on ESC-10
Vanilla gradient [35]	15.5 (8.1)
Smooth-grad [27]	23.2 (6.7)
Integrated gradients [25]	20.1 (6.5)
Input x gradient [37]	19.1 (8.7)
GradCAM [30]	24.4 (11.9)
Guided GradCAM [30]	19.4 (4.6)
GradCAM++ [23]	25.7 (8.2)
Occlusion [28]	20.1 (5.7)
RISE [29]	21.5 (4.5)
SHAP [39]	15.2 (3.3)
LIME [26]	17.0 (5.3)
<b>DAX-V1</b>	22.3 (4.2)
<b>DAX-V2</b>	<b>24.1 (4.3)</b>

TABLE VII

THE MEAN IOU (%) WITH ASSOCIATED STANDARD DEVIATION RESULTS FOR VARIOUS XAI METHODS ON THE AUDIO EVENT CLASSIFICATION TASK. THE DAX FRAMEWORK GIVES THE BEST IOU VALUES AMONG THE MODEL AGNOSTIC GRADIENT-FREE METHODS (LAST SET OF ROWS).

**Results:** Using the black-box, the explainability analysis is done on the spectrogram of audio samples in the test set of ESC-10. The dataset does not provide time aligned annotations of the sound events. As a way around, we augment the original audio files with noise, of duration ranging from 1-5 sec. at 10 dB signal-to-noise (SNR) ratio, randomly at both ends of the audio. The original audio segment location forms the ground truth for these explanations, and the task of XAI method is to locate the audio event in the noise-padded audio file. The IoU values (1-D measure) compute the intersection-over-union of the ground truth audio location (starting to end location of the original audio file) with XAI model’s explanation mask.

As shown in Figure 9, the DAX output explanations for spectrogram of noisy audio (figure 9(a)) only highlights the audio regions although noise was added (figure 9(b)). Also, the statistical analysis in terms of the mean IoU values using our approach (DAX) and 11 other approaches are shown in Table VII. Our approach is seen to provide the best mean IoU value, among all the model-agnostic gradient-free approaches compared for this task.

### C. Biomedical: Diagnosing COVID-19 from cough

Explainability finds one of its prominent requirement in biomedical applications. We study our approach and other existing approaches on the Coswara dataset [52], which contains cough recordings along with models trained to classify COVID and non-COVID participants.

**Task:** The task is the diagnosis of COVID-19 from respiratory sounds like cough sounds collected from COVID-19 positive and healthy individuals, as part of the Coswara project [52].

**Dataset:** The Coswara dataset [50] has sound recordings from different categories like breathing, cough, and speech. Our analysis in this work reports on the cough sound based task. The ground truth segmentation for the different sound events in the cough audio recording is obtained from sound event annotations released by Zhu et. al. [51]. This annotation provides time regions corresponding to “silence”, “inhalation”,

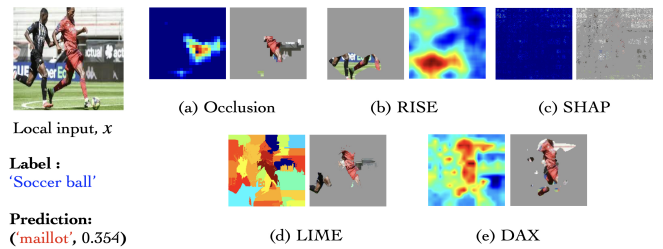


Fig. 10. Explanations  $E[x, T]$  ( $T$  : soccer ball) generated by different methods for an input sample with true label *soccer ball* which is wrongly predicted as *maillot* by the black-box. As seen, none of the XAI methods show the heat-map for the soccer ball.

“compression”, “noise”, “throat-clearing” and “cough” events in the given recording.

**Black-box:** The black-box classifier under explainability analysis is the bi-directional LSTM (BLSTM) based baseline classifier provided as part of the diagnosis of COVID-19 using acoustics (DiCOVA) challenge [53]. The model was trained on windowed segments of mel-spectrogram features and provides an area under receiver-operating-characteristics (ROC) curve of 79.8%. Similar to other tasks, we only analyze the correctly classified samples by the black-box model. A total of 73 cough samples (15 COVID positive and 58 non-COVID subjects) are evaluated in this analysis.

**Results:** In this analysis, we compare only the gradient-free methods, as shown in Table VIII. The IoU values obtained for voiced events (cough and throat clearing) are significantly higher than other unvoiced regions, which is consistently shown by all the XAI methods. Further, the DAX framework is seen to associate the model decisions of COVID/non-COVID more to the “cough” regions than the other baseline systems compared. These IoU results, along with the results reported for all the other tasks, consistently show that the proposed DAX framework is capable of explaining the model decisions for diverse tasks with state-of-art choices of black-box models.

## V. DISCUSSION AND CONCLUSION

### A. Explaining Negative Samples

All the analysis reported thus far only considered samples that were correctly predicted (positive) by the black-box model. In other words, the explanation was sought for positively predicted samples. For several applications, the explanation for the samples which were inaccurately predicted (negative) by the black-box model are also equally important. For the Pascal VoC task, we apply the XAI methods on the 141 samples which are incorrectly predicted by the ViT model.

In the IoU evaluation, we compare the XAI output with the ground truth segmentation of the target class. Thus, a lower value of IoU indicates that the black-box model prediction was inaccurate as the model was focussing on the less salient regions of the image. The mean IoU results for explaining these negative samples is reported in Table IX. As seen here, all the models see a degradation in the mean IoU values compared to the ones seen for positive samples (Table II).

We expect the XAI methods to show a large deviation in IoU values for these negative samples from those which

XAI Methods	Mean IoU (%) on the COSWARA dataset [50].					
	Cough (↑)	Throat clearing (↓)	Noise (↓)	Inhale (↓)	Compress (↓)	Silence (↓)
Occlusion	32.1 (5.7)	26.7 (5.4)	22.5 (3.5)	16.3 (2.5)	8.1 (4.2)	<b>4.1</b> (1.9)
RISE [29]	42.3 (4.5)	26.5 (5.5)	24.6 (4.9)	13.5 (3.9)	<b>6.2</b> (2.5)	6.1 (2.2)
SHAP [39]	33.5 (3.3)	21.9 (3.8)	25.1 (3.1)	19.3 (4.1)	7.5 (4.4)	5.2 (2.4)
LIME [26]	36.4 (6.3)	<b>16.8</b> (3.4)	23.2 (5.8)	18.3 (3.1)	7.1 (2.3)	5.1 (1.9)
<b>DAX-V1</b>	46.4 (5.2)	25.1 (4.3)	<b>20.2 (4.1)</b>	12.3 (4.2)	7.4 (3.5)	5.9 (2.1)
<b>DAX-V2</b>	<b>48.1 (4.9)</b>	23.6 (4.1)	21.8 (3.6)	<b>9.6 (3.8)</b>	8.1 (3.1)	4.3 (2.8)

TABLE VIII

THE MEAN IOU VALUES WITH STANDARD DEVIATION FOR THE PROPOSED (DAX) FRAMEWORK AND OTHER GRADIENT-FREE MODEL AGNOSTIC XAI METHODS. THE GROUND-TRUTH REFERENCE OF THESE AUDIO RECORDINGS IS OBTAINED FROM MANUAL ANNOTATION [51]. THE DAX APPROACH IS SHOWN TO PROVIDE THE EXPLANATION FOR THE COVID-19 CLASSIFICATION BY THE BLACK-BOX MODEL PRIMARILY BASED ON COUGH REGIONS.

Explainability Methods	Mean IoU (%) (↓)	Mean difference from accurate predictions (↑)
Occlusion [28]	18.9 (14.5)	9.6
RISE [29]	19.7 (14.2)	11.4
SHAP [39]	13.6 (10.0)	5.7
LIME [26]	16.6 (13.2)	10.2
<b>DAX-V1</b>	16.2 (13.9)	15.2
<b>DAX-V2</b>	<b>16.0 (13.6)</b>	<b>15.4</b>

TABLE IX

MEAN IOU VALUES WITH STANDARD DEVIATION OBTAINED USING EXPLANATIONS GENERATED FOR 141 INCORRECTLY PREDICTED IMAGES USING GROUND TRUTH LABELS AS TARGET CLASS. THE IOU FOR THESE SAMPLES ARE EXPECTED TO BE LOWER, WHICH MAY EXPLAIN THE BLACK-BOX MODEL’S INABILITY TO PREDICT THE CORRECT CLASS.

are positively classified. The mean IoU difference between positive and negative samples is also shown in this Table. The SHAP model generates the lowest IoU results for these evaluations. However, the mean difference is considerably small, indicating that the SHAP model does not allow a strong distinction between positive and negative samples. Among all the gradient-free post-hoc explainability methods, the DAX framework has the highest difference in IoU values between positive and negative samples, indicating that the XAI method is also applicable for explaining wrong decisions by the black-box model. An illustrative example of explaining a negative sample is also shown in Figure 10.

### B. Summary

This paper proposes an approach for post-hoc gradient-free explainability, called distillation aided explanations (DAX). The DAX framework poses model explanations as a learnable function, given the input sample, its perturbed versions and the corresponding black-box model outputs. Without gradient access, the learning of the DAX function is achieved using a distilled student network that locally approximates the black-box model. Both the masking network and the distillation are jointly optimized to generate the explanation function.

The DAX framework is evaluated on image and audio sub-tasks with state-of-art black box models. The qualitative examples show that the DAX framework generates consistent explanations for wide variety of image classes (Figure 6). Further, quantitative evaluations are performed by comparing the model explanations with ground truth segments of the

objects/audio-events, for the correctly classified samples. The experiments on diverse audio and image tasks explored in this paper illustrate the benefits of DAX framework in comparison with a variety of other XAI benchmarks.

## VI. ACKNOWLEDGEMENT

This work was supported by grants from Verisk Analytics as well as grants from Qualcomm Innovation Fellowship. We are grateful to Maneesh Singh, Chayan Sharma and Rahul Mitra for the valuable feedback during the conduct of this work.

## REFERENCES

- [1] Yann LeCun, Yoshua Bengio, and Geoffrey Hinton, “Deep learning,” *nature*, vol. 521, no. 7553, pp. 436–444, 2015.
- [2] Sepp Hochreiter and Jürgen Schmidhuber, “Long short-term memory,” *Neural computation*, vol. 9, no. 8, pp. 1735–1780, 1997.
- [3] Dzmitry Bahdanau, Kyunghyun Cho, and Yoshua Bengio, “Neural machine translation by jointly learning to align and translate,” in *3rd International Conference on Learning Representations, ICLR 2015, San Diego, CA, USA, May 7-9, 2015, Conference Track Proceedings*, Yoshua Bengio and Yann LeCun, Eds., 2015.
- [4] Ashish Vaswani, Noam Shazeer, Niki Parmar, Jakob Uszkoreit, Llion Jones, Aidan N Gomez, Łukasz Kaiser, and Illia Polosukhin, “Attention is all you need,” *Advances in neural information processing systems*, vol. 30, 2017.
- [5] David E Rumelhart, Geoffrey E Hinton, and Ronald J Williams, “Learning internal representations by error propagation,” Tech. Rep., California Univ San Diego La Jolla Inst for Cognitive Science, 1985.
- [6] Alexey Dosovitskiy, Lucas Beyer, Alexander Kolesnikov, Dirk Weissenborn, Xiaohua Zhai, Thomas Unterthiner, Mostafa Dehghani, Matthias Minderer, Georg Heigold, Sylvain Gelly, et al., “An image is worth 16x16 words: Transformers for image recognition at scale,” *arXiv preprint arXiv:2010.11929*, 2020.
- [7] Alec Radford, Jong Wook Kim, Tao Xu, Greg Brockman, Christine McLeavey, and Ilya Sutskever, “Robust speech recognition via large-scale weak supervision,” *arXiv preprint arXiv:2212.04356*, 2022.
- [8] OpenAI, “GPT-4 technical report,” *arXiv*, vol. 2303.08774, 2023.
- [9] Jianping Gou, Xiangshuo Xiong, Baosheng Yu, Lan Du, Yibing Zhan, and Dacheng Tao, “Multi-target knowledge distillation via student self-reflection,” *International Journal of Computer Vision*, vol. 131, no. 7, pp. 1857–1874, 2023.
- [10] Jianping Gou, Liyuan Sun, Baosheng Yu, Shaohua Wan, Weihua Ou, and Zhang Yi, “Multilevel attention-based sample correlations for knowledge distillation,” *IEEE Transactions on Industrial Informatics*, vol. 19, no. 5, pp. 7099–7109, 2022.
- [11] Shachar Kaufman, Saharon Rosset, Claudia Perlich, and Ori Stitelman, “Leakage in data mining: Formulation, detection, and avoidance,” *ACM Transactions on Knowledge Discovery from Data (TKDD)*, vol. 6, no. 4, pp. 1–21, 2012.
- [12] Kayur Patel, James Fogarty, James A Landay, and Beverly Harrison, “Investigating statistical machine learning as a tool for software development,” in *Proceedings of the SIGCHI Conference on Human Factors in Computing Systems*, 2008, pp. 667–676.

- [13] “ChatGPT,” 2022.
- [14] Finale Doshi-Velez, Mason Kortz, Ryan Budish, Chris Bavitz, Sam Gershman, David O’Brien, Kate Scott, Stuart Schieber, James Waldo, David Weinberger, et al., “Accountability of AI under the law: The role of explanation,” *arXiv preprint arXiv:1711.01134*, 2017.
- [15] Zachary C Lipton, “The myths of model interpretability: In machine learning, the concept of interpretability is both important and slippery,” *Queue*, vol. 16, no. 3, pp. 31–57, 2018.
- [16] Andreas Holzinger, Chris Biemann, Constantinos S Pattichis, and Douglas B Kell, “What do we need to build explainable AI systems for the medical domain?,” *arXiv preprint arXiv:1712.09923*, 2017.
- [17] Rich Caruana, Yin Lou, Johannes Gehrke, Paul Koch, Marc Sturm, and Noemie Elhadad, “Intelligible models for healthcare: Predicting pneumonia risk and hospital 30-day readmission,” in *Proceedings of the 21th ACM SIGKDD international conference on knowledge discovery and data mining*, 2015, pp. 1721–1730.
- [18] Q Vera Liao, Daniel Gruen, and Sarah Miller, “Questioning the AI: informing design practices for explainable AI user experiences,” in *Proceedings of the 2020 CHI Conference on Human Factors in Computing Systems*, 2020, pp. 1–15.
- [19] Alexandra Chouldechova and Aaron Roth, “A snapshot of the frontiers of fairness in machine learning,” *Communications of the ACM*, vol. 63, no. 5, pp. 82–89, 2020.
- [20] Gabrielle Ras, Ning Xie, Marcel van Gerven, and Derek Doran, “Explainable deep learning: A field guide for the uninitiated,” *Journal of Artificial Intelligence Research*, vol. 73, pp. 329–397, 2022.
- [21] Fulton Wang and Cynthia Rudin, “Causal falling rule lists,” *arXiv preprint arXiv:1510.05189*, 2015.
- [22] Bolei Zhou, Aditya Khosla, Agata Lapedriza, Aude Oliva, and Antonio Torralba, “Learning deep features for discriminative localization,” in *Proceedings of the IEEE conference on computer vision and pattern recognition*, 2016, pp. 2921–2929.
- [23] Aditya Chattopadhyay, Anirban Sarkar, Prantik Howlader, and Vineeth N Balasubramanian, “Grad-CAM++: Generalized gradient-based visual explanations for deep convolutional networks,” in *2018 IEEE winter conference on applications of computer vision (WACV)*. IEEE, 2018, pp. 839–847.
- [24] Daniel Smilkov, Nikhil Thorat, Been Kim, Fernanda B. Viégas, and Martin Wattenberg, “Smoothgrad: removing noise by adding noise,” *CoRR*, vol. abs/1706.03825, 2017.
- [25] Mukund Sundararajan, Ankur Taly, and Qiqi Yan, “Axiomatic attribution for deep networks,” in *International conference on machine learning*. PMLR, 2017, pp. 3319–3328.
- [26] Marco Tulio Ribeiro, Sameer Singh, and Carlos Guestrin, ““why should I trust you?” explaining the predictions of any classifier,” in *Proceedings of the 22nd ACM SIGKDD international conference on knowledge discovery and data mining*, 2016, pp. 1135–1144.
- [27] Daniel Smilkov, Nikhil Thorat, Been Kim, Fernanda Viégas, and Martin Wattenberg, “Smoothgrad: removing noise by adding noise,” *arXiv preprint arXiv:1706.03825*, 2017.
- [28] Matthew D Zeiler and Rob Fergus, “Visualizing and understanding convolutional networks,” in *European conference on computer vision*. Springer, 2014, pp. 818–833.
- [29] Vitali Petsiuk, Abir Das, and Kate Saenko, “RISE: Randomized input sampling for explanation of black-box models,” *arXiv preprint arXiv:1806.07421*, 2018.
- [30] Ramprasaath R Selvaraju, Michael Cogswell, Abhishek Das, Ramakrishna Vedantam, Devi Parikh, and Dhruv Batra, “Grad-CAM: Visual explanations from deep networks via gradient-based localization,” in *Proceedings of the IEEE international conference on computer vision*, 2017, pp. 618–626.
- [31] Karthikeyan Natesan Ramamurthy, Bhanukiran Vinzamuri, Yunfeng Zhang, and Amit Dhurandhar, “Model agnostic multilevel explanations,” *Advances in neural information processing systems*, vol. 33, pp. 5968–5979, 2020.
- [32] Tejaswini Pedapati, Avinash Balakrishnan, Karthikeyan Shanmugam, and Amit Dhurandhar, “Learning global transparent models consistent with local contrastive explanations,” *Advances in neural information processing systems*, vol. 33, pp. 3592–3602, 2020.
- [33] Aditya Ramesh, Mikhail Pavlov, Gabriel Goh, Scott Gray, Chelsea Voss, Alec Radford, Mark Chen, and Ilya Sutskever, “Zero-shot text-to-image generation,” in *International Conference on Machine Learning*. PMLR, 2021, pp. 8821–8831.
- [34] Debarpan Bhattacharya, Deepak Mittal, Amir Poorjam, and Sriram Ganapathy, “DAME: A Distillation Based Approach For Model-agnostic Local Explainability,” [rejected] International Conference on Learning Representations, 2023. <https://openreview.net/forum?id=EAT7gmyIH2&noteId=Nb49J50EYR>.
- [35] Karen Simonyan, Andrea Vedaldi, and Andrew Zisserman, “Visualising image classification models and saliency maps,” *Deep Inside Convolutional Networks*, 2014.
- [36] Avanti Shrikumar, Peyton Greenside, Anna Shcherbina, and Anshul Kundaje, “Not just a black box: Learning important features through propagating activation differences,” *arXiv preprint arXiv:1605.01713*, 2016.
- [37] Avanti Shrikumar, Peyton Greenside, and Anshul Kundaje, “Learning important features through propagating activation differences,” in *International conference on machine learning*. PMLR, 2017, pp. 3145–3153.
- [38] Jason Yosinski, Jeff Clune, Anh Nguyen, Thomas Fuchs, and Hod Lipson, “Understanding neural networks through deep visualization,” *arXiv preprint arXiv:1506.06579*, 2021.
- [39] Scott M Lundberg and Su-In Lee, “A unified approach to interpreting model predictions,” *Advances in neural information processing systems*, vol. 30, 2017.
- [40] Nina Narodytska, Aditya Shrotri, Kuldeep S Meel, Alexey Ignatiev, and Joao Marques-Silva, “Assessing heuristic machine learning explanations with model counting,” in *International Conference on Theory and Applications of Satisfiability Testing*. Springer, 2019, pp. 267–278.
- [41] Alexander Kirillov, Eric Mintun, Nikhila Ravi, Hanzi Mao, Chloe Rolland, Laura Gustafson, Tete Xiao, Spencer Whitehead, Alexander C Berg, Wan-Yen Lo, et al., “Segment anything,” in *Proceedings of the IEEE/CVF International Conference on Computer Vision*, 2023, pp. 4015–4026.
- [42] Ruth C Fong and Andrea Vedaldi, “Interpretable explanations of black boxes by meaningful perturbation,” in *Proceedings of the IEEE international conference on computer vision*, 2017, pp. 3429–3437.
- [43] Andrea Vedaldi and Stefano Soatto, “Quick shift and kernel methods for mode seeking,” in *Computer Vision—ECCV 2008: 10th European Conference on Computer Vision, Marseille, France, October 12–18, 2008, Proceedings, Part IV 10*. Springer, 2008, pp. 705–718.
- [44] Jia Deng, Wei Dong, Richard Socher, Li-Jia Li, Kai Li, and Li Fei-Fei, “Imagenet: A large-scale hierarchical image database,” in *2009 IEEE conference on computer vision and pattern recognition*. Ieee, 2009, pp. 248–255.
- [45] Alexey Dosovitskiy, Lucas Beyer, Alexander Kolesnikov, Dirk Weissenborn, Xiaohua Zhai, Thomas Unterthiner, Mostafa Dehghani, Matthias Minderer, Georg Heigold, Sylvain Gelly, Jakob Uszkoreit, and Neil Houlsby, “An image is worth 16x16 words: Transformers for image recognition at scale,” in *International Conference on Learning Representations*, 2021.
- [46] Mark Everingham, SM Eslami, Luc Van Gool, Christopher KI Williams, John Winn, and Andrew Zisserman, “The Pascal visual object classes challenge: A retrospective,” *International journal of computer vision*, vol. 111, no. 1, pp. 98–136, 2015.
- [47] Kaiming He, Xiangyu Zhang, Shaoqing Ren, and Jian Sun, “Deep residual learning for image recognition,” in *Proceedings of the IEEE conference on computer vision and pattern recognition*, 2016, pp. 770–778.
- [48] Sunnie SY Kim, Nicole Meister, Vikram V Ramaswamy, Ruth Fong, and Olga Russakovsky, “Hive: Evaluating the human interpretability of visual explanations,” in *European Conference on Computer Vision*. Springer, 2022, pp. 280–298.
- [49] Karol J Piczak, “ESC: Dataset for environmental sound classification,” in *Proceedings of the 23rd ACM international conference on Multimedia*, 2015, pp. 1015–1018.
- [50] Debarpan Bhattacharya, Neeraj Kumar Sharma, Debottam Dutta, Srikanth Raj Chetupalli, Pravin Mote, Sriram Ganapathy, C Chandrakiran, Sahiti Nori, KK Suhail, Sadhana Gonuguntla, et al., “Coswara: A respiratory sounds and symptoms dataset for remote screening of sars-cov-2 infection,” *Scientific Data*, vol. 10, no. 1, pp. 397, 2023.
- [51] Yi Zhu, Mahil Hussain Shaik, and Tiago H Falk, “On the importance of different cough phases for covid-19 detection,” in *ICASSP 2023-2023 IEEE International Conference on Acoustics, Speech and Signal Processing (ICASSP)*. IEEE, 2023, pp. 1–5.
- [52] “Coswara web link,” <https://coswara.iisc.ac.in/>, Last Accessed May, 2023.
- [53] Neeraj Kumar Sharma, Srikanth Raj Chetupalli, Debarpan Bhattacharya, Debottam Dutta, Pravin Mote, and Sriram Ganapathy, “The second DICOVA challenge: Dataset and performance analysis for diagnosis of covid-19 using acoustics,” in *IEEE International Conference on Acoustics, Speech and Signal Processing (ICASSP)*. IEEE, 2022, pp. 556–560.